Crossed beam reaction of cyano radicals with hydrocarbon molecules. I. Chemical dynamics of cyanobenzene (C_6H_5CN; X^1A_1) and perdeutero cyanobenzene (C_6D_5CN; X^1A_1) formation from reaction of $CN(X^2\Sigma^+)$ with benzene $C_6H_6(X^1A_{1g})$, and d_6-benzene $C_6D_6(X^1A_{1g})$

N. Balucani,[a] O. Asvany,[b] A. H. H. Chang, S. H. Lin, Y. T. Lee, and R. I. Kaiser[b,c]
Institute of Atomic and Molecular Sciences, 1, Section 4, Roosevelt Road, 107 Taipei, Taiwan, Republic of China

H. F. Bettinger,[d] P. v. R. Schleyer, and H. F. Schaefer III
Center for Computational Quantum Chemistry, The University of Georgia, Athens, Georgia 30602

(Received 2 June 1999; accepted 28 July 1999)

The chemical reaction dynamics to form cyanobenzene $C_6H_5CN(X\,^1A_1)$, and perdeutero cyanobenzene $C_6D_5CN(X\,^1A_1)$ via the neutral–neutral reaction of the cyano radical $CN(X\,^2\Sigma^+)$, with benzene $C_6H_6(X\,^1A_{1g})$ and perdeutero benzene $C_6D_6(X\,^1A_{1g})$, were investigated in crossed molecular beam experiments at collision energies between 19.5 and 34.4 kJ mol^{-1}. The laboratory angular distributions and time-of-flight spectra of the products were recorded at mass to charge ratios $m/e=103-98$ and 108–98, respectively. Forward-convolution fitting of our experimental data together with electronic structure calculations (B3LYP/6−311+G**) indicate that the reaction is without entrance barrier and governed by an initial attack of the CN radical on the carbon side to the aromatic π electron density of the benzene molecule to form a C_s symmetric $C_6H_6CN(C_6D_6CN)$ complex. At all collision energies, the center-of-mass angular distributions are forward–backward symmetric and peak at $\pi/2$. This shape documents that the decomposing intermediate has a lifetime longer than its rotational period. The H/D atom is emitted almost perpendicular to the C_6H_5CN plane, giving preferentially sideways scattering. This experimental finding can be rationalized in light of the electronic structure calculations depicting a H–C–C angle of 101.2° in the exit transition state. The latter is found to be tight and located about 32.8 kJ mol^{-1} above the products. Our experimentally determined reaction exothermicity of 80–95 kJ mol^{-1} is in good agreement with the theoretically calculated one of 94.6 kJ mol^{-1}. Neither the C_6H_6CN adduct nor the stable iso cyanobenzene isomer C_6H_5NC were found to contribute to the scattering signal. The experimental identification of cyanobenzene gives a strong background for the title reaction to be included with more confidence in reaction networks modeling the chemistry in dark, molecular clouds, outflow of dying carbon stars, hot molecular cores, as well as the atmosphere of hydrocarbon rich planets and satellites such as Saturn's moon Titan. This reaction might further present a barrierless route to the formation of heteropolycyclic aromatic hydrocarbons via cyanobenzene in these extraterrestrial environments as well as hydrocarbon rich flames. © *1999 American Institute of Physics.* [S0021-9606(99)00940-X]

I. INTRODUCTION

The chemical reaction dynamics of free radical reactions are of great relevance in a wide variety of chemical processes such as combustion, plasmas, atmospheric processes,[1] as well as in the chemistry of extraterrestrial environments such as molecular clouds and the outflow of carbon stars.[2] Understanding their reaction mechanisms requires an intimate knowledge of the involved elementary processes at the most fundamental microscopic level. The crossed molecular beam technique[3] represents a versatile tool to unravel these chemical reaction dynamics, triply differential cross sections, pertinent intermediates (if any), and reaction products. These experiments are conducted under well-characterized primary and secondary beam conditions with narrow velocity distributions, well-defined interaction angle, and consequently well-defined collision energy. Most important, these investigations are performed under single collision conditions precluding subsequent collisions that could modify the nature of the primary products or their energy content.

In order to perform a crossed beam experiment on radi-

[a]Visiting scientist, Permanent address: Dipartimento di Chimica, Università di Perugia, 06123 Perugia, Italy.
[b]Also at: Department of Physics, Technical University Chemnitz-Zwickau, 09107 Chemnitz, Germany.
[c]Author to whom correspondence should be addressed. Electronic mail: kaiser@po.iams.sinica.edu.tw
[d]Author to whom correspondence should be addressed. Electronic mail: bettingr@paul.chem.uga.edu

cal reactions, because of the low efficiency of the scattering event, one stringent requirement is the generation of a radical beam of sufficiently high concentration to guarantee a detectable quantity of final products and a reasonable signal-to-noise ratio. Different methods have been used to generate radicals, such as photolysis, pyrolysis, plasma source and chemical reactions, or other collision induced processes. Nevertheless, the reaction dynamics have been elucidated so far only for a few simple tetratomic systems, namely the reaction of cyano $CN(X\,^2\Sigma^+)$ with D_2,[4] and O_2,[5] hydroxyl $OH(X\,^2\Pi)$ with H_2,[6] and CO,[7] and methylidene $CH(X\,^2\Pi)$ with D_2.[8] Among polyatomic systems, the reactive scattering of pyrolytically generated methyl radicals, $CH_3(X\,^2A_2'')$, with iodoalkanes[9] has been investigated. Most recently, crossed beam experiments of the phenyl radical $C_6H_5(X\,^2A_1)$, with methylacetylene CH_3CCH,[10] as well as the atom–radical reactions involving atomic carbon $C(^3P_j)$ and propargyl, $C_3H_3(X\,^2B_2)$,[11] and vinyl $C_2H_3(X\,^2A')$,[12] have been reported.

Among these free radical reactions, those of cyano radicals $CN(X\,^2\Sigma^+)$ are known to play a significant role in the chemistry of numerous interesting extraterrestrial environments such as interstellar clouds,[13] comets, and planetary atmospheres of the saturnian satellite Titan.[14] Reactions of cyano radicals are also of relevance in the combustion chemistry of nitrogen-containing fuels. From a fundamental point of view the reactions of CN radicals are intriguing as well: the carbon–nitrogen triple bond is very strong and the radical has a large electronic affinity. Because of that it has often been called a pseudo- or superhalogen and in most reactions the carbon–nitrogen bond remains intact. However CN is a diatomic radical and this may imply a different chemical behavior than fluorine or chlorine. For instance, an obvious difference is that CN can be internally excited and that may or may not influence its chemical properties.

The reactions of CN with simple unsaturated hydrocarbons are specifically interesting in astrochemistry and, because of that, numerous studies of CN reactions with unsaturated molecules have been performed by exploiting the most modern conventional kinetic techniques. For instance, recent laboratory measurements at temperatures as low as 15 K show that the rate constants of CN reactions with acetylene and ethylene increases as the temperature decreases, reaching a maximum of $5\times10^{-10}\,cm^3\,s^{-1}$ at 30 K, pointing to a very high reactivity of these systems also in extreme environments.[15] The reaction rate constant for the reaction of CN radicals with benzene was measured to be $2.8\times10^{-10}\,cm^3\,s^{-1}$, but the authors interpreted this result in light of a hydrogen atom abstraction to form HCN and a phenyl radical.[16] However, these studies can monitor only the decay kinetics of the CN radical, and hence reaction products could not be determined explicitly. This shortcoming clearly reveals that systematic experiments are necessary to probe the detailed chemical dynamics and reaction product(s) of the title reaction under single collision conditions. Hitherto, the reaction mechanism has been elucidated experimentally and theoretically, so far, only for the simplest CN radical reaction, that with molecular hydrogen.[4] Experiments and quasiclassical trajectory calculations indicate that the reaction dynamics are governed by a direct abstraction mechanism at low collision energies. This system may be regarded as a prototype for CN reactions because of its simplicity; however, the reaction mechanism with unsaturated hydrocarbons is expected to be different, with the addition of CN to the π system being dominant. Here, recent studies of one of the simplest CN reaction with unsaturated hydrocarbons, that of CN with acetylene, C_2H_2, documented the existence of a CN versus H exchange channel to form cyano acetylene HCCCN.[17]

The present paper is the first in a series of a systematic and detailed investigations on the chemical reaction dynamics of $CN(X\,^2\Sigma^+)$ radical reactions with unsaturated and aromatic hydrocarbons. All experiments were performed under single collision conditions employing the crossed molecular beam technique.[18] These studies were supplemented by electronic structure calculations. The paper is laid out as follows: Secs. II and III describe the experimental setup, data processing, and the electronic structure calculations. Section IV focus as on the laboratory angular distributions, time-of-flight data, and the derived center-of-mass functions together with the flux contour maps. Section V discusses the involved potential energy surfaces as obtained from our theoretical investigations and compares the experimental findings with the theoretical results. Crossed beam experiments of the related $F+C_6H_6$ system are discussed in detail as well. Finally, astrophysical implications and solar system applications are given in the remaining sections.

II. EXPERIMENT AND DATA PROCESSING

The 35 in. crossed molecular beam machine used here consists of two source chambers fixed at a 90° crossing angle (10^{-4}–10^{-5} mbar during the experiments), a stainless steel scattering chamber (10^{-7} mbar), and a rotatable, triply differentially pumped quadrupole mass spectrometric detector (10^{-11} mbar). The scattering chamber is evacuated by two $2000\,\ell\,s^{-1}$ magnetically levitated, oil free turbomolecular pumps, backed by an oil free $500\,\ell\,s^{-1}$ scroll pump. The primary and secondary beam sources are placed in separate, removable side chambers each pumped by 2000 and $400\,\ell\,s^{-1}$ magnetically levitated turbomolecular pumps. Both pumps are backed by a roots blower and mechanical pump. Rapidly responding gate valves located between the exhaust lines of each turbomolecular and roughing pump are interlocked via a convectron gauge close to the inlet flange of the backing pump. These valves are shut automatically in the case of power failure or pump breakdown.

A pulsed supersonic cyano $CN(X\,^2\Sigma^+)$ radical beam is generated in the primary source *in situ* via laser ablation of graphite at 266 nm.[19,20] Neat nitrogen is used as a carrier and reactant gas and released by a Proch–Trickl pulsed valve (1.0 mm nozzle diameter) which is driven at −600 V with 60 Hz, 80 μs pulses, and 4 atm backing pressure.[21] The Spectra Physics GCR 270–30 Nd-YAG laser operates at 30 Hz; 30 mJ per pulse are focused onto a rotating graphite rod to a

TABLE I. Experimental beam conditions and 1σ errors: most probable velocity v_p, speed ratio S, most probable collision energy with the benzene molecules E_{coll}, and center-of-mass angles θ_{CM}.

Experiment	v_p (ms^{-1})	S	E_{coll} (kJ mol^{-1})	θ_{CM}
CN/C_6H_6	1720±10	4.6±0.2	34.4±0.4	52.8±0.5
CN/C_6H_6	1590±10	4.8±0.3	30.6±0.2	55.8±0.5
CN/C_6D_6	1185±10	6.0±0.2	19.5±0.5	63.9±0.4
Ne/C_6H_6	780±10	12.3±0.2	-	-
Ne/C_6D_6	750±10	12.2±0.2	-	-

spot of 0.3–0.5 mm diameter. Higher laser powers are found to form vibrationally excited CN radicals.[20] The laser beam port is differentially pumped by an oil free pumping station and completely isolated from the second source region to avoid reaction of CN radicals with background reactant molecules. After the pulsed CN beam passes the skimmer of 1.0 mm diameter, a four-slot chopper wheel mounted 40 mm after the ablation zone selects a 9.0 μs segment of the pulse. This segment and the second, pulsed supersonic benzene C_6H_6 or perdeutero benzene C_6D_6 seeded in neon carrier gas cross at 90° with divergencies of 3.0° and 4.3° under a well-defined collision energy in the interaction region (Table I). The second pulsed valve has a nozzle diameter of 0.75 mm and is operated at −500 V with 60 Hz, 80 μs pulses, and 620–630 Torr backing pressure. Self-attenuation of both supersonic beams due to nozzle–skimmer interferences[22] was minimized by optimizing the nozzle–skimmer distance in the primary and secondary source to 18 and 16 mm, respectively. To avoid any reaction of CN radicals with benzene clusters present in the slower part of the secondary beam, extreme care has to be given to choose the correct time delay between both pulsed valves. In our experiments, the second pulsed valve opens about 15–20 μs prior to the primary pulsed valve to allow the fast part of the benzene beam to cross with the CN pulse.

Reactively scattered species are monitored between 10.0° and 72.0° using a differentially pumped quadrupole mass spectrometer,[23] rotatable in the plane of the beams with respect to the interaction region. Differentially pumped regions I and II reduce the gas load from the main chamber, whereas region III contains the Brink-type electron impact ionizer,[24] surrounded by a liquid nitrogen cold shield, the quadrupole mass filter, and the Daly-type scintillation particle detector.[25] Each region is pumped by a magnetically levitated turbomolecular pump ($400\,\ell\,s^{-1}$); all three pumps are backed by a fourth $400\,\ell\,s^{-1}$ turbomolecular pump whose exhaust is connected to an oil free pumping station which consists of a molecular drag and a membrane pump. This pumping scheme gives about $1-2\times10^{-11}$ Torr in region III. A slide valve with an O-ring is used to separate the reaction chamber from the first differentially pumped detector region: during on-axis operation a small detector aperture of 0.23 mm is applied, whereas off-beam-axis reactive scattering experiments require a larger, 3.8 mm×3.8 mm rectangular aperture. Two 5.8 mm×5.8 mm rectangles constrain the viewing angle of the ionizer nested 34.3 cm from the interaction region to 0.94° in each direction. The ionizer consists of a thoriated iridium filament[26] spot welded to a gold plated stainless steel cylindrical can, a meshed wire grid, and an extractor lens held at −800 V. The electron energy, i.e., the potential difference between the can and the grid, was optimized to 200 eV, whereas the ion energy was held at +80 eV. Extracted ions are focused by an electric lens located after the extractor plate and pass the quadrupole mass filter and are accelerated towards a stainless steel target maintained at −25 kV. The ion hits the surface and initiates an electron cascade which is accelerated by the same potential until they reach an organic scintillator whose photon cascade is detected by a photomultiplier tube (PMT) mounted outside the ultrahigh vacuum detector and held between 1500 and 1700 V. Each PMT pulse is amplified and passes a discriminator to eliminate low-level noise. After conversion from NIM- to TTL standard the signal is fed into the multichannel scaler I and II (dwell time of each channel between 5 and 10.0 μs).

Despite the detector differential pumping setup described above, molecules desorbing from wall surfaces lying on a straight line to the electron impact ionizer (straight-through molecules) cannot be avoided since the mean free path of these species is on the order of 10^3 m compared to maximum detector dimensions of about 1 m. To reduce this background contribution, right before the collision center a copper plate attached to a two stage closed cycle helium refrigerator and cooled down to 4.5 K is placed. Since the copper shield is located between the two skimmers and the scattering region, the ionizer ''views'' a cooled surface which traps all the species with the exception of H_2 and He.

The velocity distribution of the products was recorded using the time-of-flight (TOF) method. Information on the chemical dynamics of the reaction was gained by fitting the TOF spectra and the product angular-distribution in the laboratory frame (LAB) using a forward-convolution routine.[27] This trial and error procedure initially assumes an angular distribution $T(\theta)$ and a translational energy distribution $P(E_T)$ in the center-of-mass (CM) reference frame. Laboratory TOF spectra and (the laboratory) angular distributions were then calculated from $T(\theta)$ and $P(E_T)$ accounting for the transformation Jacobian and averaging over the apparatus and beam functions. Best TOF and (LAB) angular distributions were achieved by iteratively refining adjustable $T(\theta)$ and $P(E_T)$ parameters. The ultimate outcome is the generation of a product flux contour map which reports the differential cross section, $I(\theta,u)\sim P(u)*T(\theta)$, as the intensity, as a function of angle θ and product CM velocity u. This map serves as an image of the reaction and contains all the information of the scattering process.

III. ELECTRONIC STRUCTURE AND RICE–RAMSPERGER–KASSEL–MARCUS (RRKM) CALCULATIONS

The theoretical investigation was performed at the hybrid Hartree–Fock/density functional level of theory using Becke's[28] three-parameter hybrid functional together with the correlation functional of Lee *et al.*[29] as implemented in

GAUSSIAN 94.[30] The 6-311+G** basis set was employed for geometry optimization on the computation of harmonic vibrational frequencies at stationary points. The spin unrestricted formalism was employed for all open-shell species. The vibrational frequencies and the zero point vibrational energies (ZPVEs) are unscaled. All data reported were obtained at the B3LYP/6-311+G**+ZPVE level of theory.

According to the quasiequilibrium theory of RRKM theory,[31] the rate constant $k(E)$ at a collision energy E for a unimolecular reaction $A^* \rightarrow A^\ddagger \rightarrow P$ can be expressed as

$$k(E) = \frac{\sigma}{h} \cdot \frac{W^\ddagger(E-E^\ddagger)}{\rho(E)}, \quad (1)$$

where σ is the symmetry factor, $W^\ddagger(E-E^\ddagger)$ denotes the total number of states of the transition state (activated complex) $A^\ddagger$ with the barrier $E^\ddagger$, $\rho(E)$ represents the density of states of the energized reactant molecule A^*, and P is the product or products. The harmonic oscillator and rigid rotor approximation were assumed for the species involved throughout the rate constant calculations. The saddle point method was applied to evaluate $\rho(E)$ and $W(E)$. A simple scheme,[32] where an inverted parabola was used for the barrier along the reaction coordinate, was also employed to incorporate the tunneling corrections to the RRKM rate constant k_2.

IV. RESULTS

A. Reactive scattering signal

We observed reactive scattering signals at mass to charge ratios $m/e = 103-98$, i.e., $C_6H_5CN^+$ to C_7N^+, and 108–103 in case of perdeutero benzene at all three collision energies of 19.5, 30.6, and 34.4 kJ mol^{-1}, TOF spectra taken at selected angles depicting identical patterns and could be fit with the same CM functions, indicating that the signal at lower m/e ratios originates in cracking of the parent in the electron impact ionizer. Therefore, all TOF spectra were recorded at the most intense fragments $m/e = 102$ (C_6H_6+CN experiment) and 107 (C_6D_6+CN experiment). In addition, no radiative association channels to C_6H_6+CN ($m/e = 104$) or the deuterated counterpart were detected. Due to the high background level at $m/e = 27$ we were unable to detect a possible HCN or HNC reaction product from an H abstraction reaction.

B. Laboratory angular distributions (LAB) and TOF spectra

Figures 1–3 show the most probable Newton diagrams of the reaction $CN(X\,^2\Sigma^+) + C_6D_6(X\,^1A_{1g}) \rightarrow C_6D_5CN(X\,^1A_1) + D(^2S_{1/2})$ and $CN(X\,^2\Sigma^+) + C_6H_6(X\,^1A_{1g}) \rightarrow C_6H_5CN(X\,^1A_1) + H(^2S_{1/2})$ together with the laboratory product angular distributions and the calculated curves using the CM best fit functions. TOF spectra are shown in Figs. 4–6. All LAB distributions peak very close to the cm angles of 63.9°, 55.8°, and 52.8°, and are very narrow. The reactive scattering products are spread to less than 40° in the scattering plane. If we compare these scattering

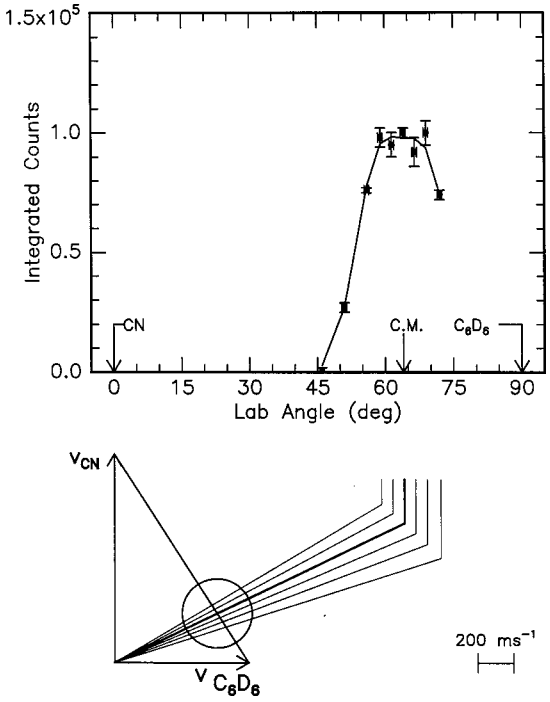

FIG. 1. Lower: Newton diagram for the reaction $CN(X\,^2\Sigma^+) + C_6D_6(X\,^1A_{1g}) \rightarrow C_6D_5CN(X\,^1A_1) + D(^2S_{1/2})$ at a collision energy of 19.5 kJ mol^{-1}. The circle stands for the maximum center-of-mass recoil velocity of the C_6D_5CN product assuming all the available energy is released as translational energy. Upper: Laboratory angular distribution of the $C_6D_5CN(X\,^1A_1)$ product. Circles and error bars indicate experimental data, and the solid line indicates the calculated distribution.

ranges with the limiting Newton circles of the C_6H_5CN and its deuterated counterpart, it is apparent that the thermodynamically more stable C_6H_5CN is predominantly formed. The larger Newton circle of the deuterated reaction is simply based on the different kinematics due to the different mass combinations of the products, i.e., masses 2 and 108 versus masses 1 and 103. This translates into a better resolution of the TOF spectra of the reaction $CN(X\,^2\Sigma^+) + C_6D_6(X\,^1A_{1g})$ and more pronounced shoulders in those spectra at angles between 59.0° and 69.0°.

C. Center-of-mass translational energy distribution $P(E_T)$

All data could be fitted assuming that one single reaction channel is responsible for the observed distributions. The best-fit CM functions are presented in Figs. 7–12. All functions shown are within the upper and lower experimental error limits of the LAB data. The best fit $P(E_T)$ energy tails extend up to an energy maximum E_{max} of 90–110 kJ mol^{-1} (Fig. 7), 110–112 kJ mol^{-1} (Fig. 8), and 110–118 kJ mol^{-1} (Fig. 9). The fits of the laboratory data do not change if the $P(E_T)$ are extended or shortened by 15 kJ mol^{-1}. If we account for the collision energies, we found a reaction exothermicity of about 70–90, 80–81, and 75–84 kJ mol^{-1}, using the three different sets of data. Since the energetics to form the C_6H_5CN and C_6H_5NC isomer are well separated with reaction exothermicities of 94.6 and 4.9 kJ mol^{-1} as based on our calculations, we can use E_{max} to identify the product

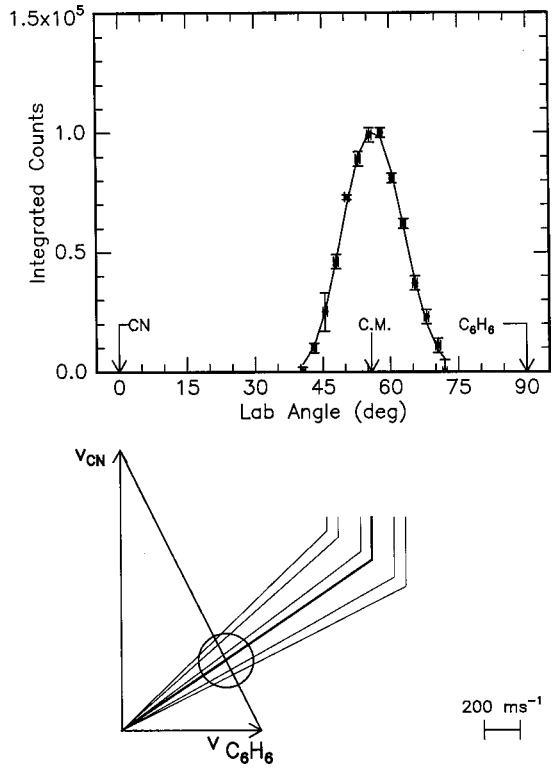

FIG. 2. Lower: Newton diagram for the reaction $CN(X\,^2\Sigma^+) + C_6H_6(X\,^1A_{1g}) \rightarrow C_6H_5CN(X\,^1A_1) + H(^2S_{1/2})$ at a collision energy of 30.6 kJ mol^{-1}. The circle stands for the maximum center-of-mass recoil velocity of the C_6H_5CN product assuming all the available energy is released as translational energy. Upper: Laboratory angular distribution of the $C_6H_5CN(X\,^1A_1)$ product. Circles and error bars indicate experimental data, and the solid line indicates the calculated distribution.

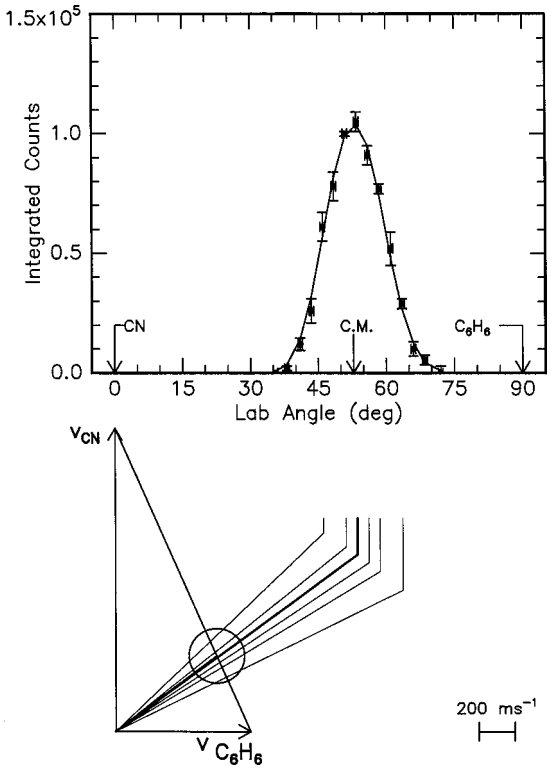

FIG. 3. Lower: Newton diagram for the reaction $CN(X\,^2\Sigma^+) + C_6H_6(X\,^1A_{1g}) \rightarrow C_6H_5CN(X\,^1A_1) + H(^2S_{1/2})$ at a collision energy of 34.4 kJ mol^{-1}. The circle stands for the maximum center-of-mass recoil velocity of the C_6H_5CN product assuming all the available energy is released as translational energy. Upper: Laboratory angular distribution of the $C_6H_5CN(X\,^1A_1)$ product. Circles and error bars indicate experimental data, and the solid line the calculated distribution.

isomer. It is obvious that at least the more stable C_6H_5CN isomer is formed as already suggested by the LAB distributions. Based on these data alone, we cannot determine the contribution of C_6H_5NC yet. Further, all $P(E_T)$s peak between 25 and 38 kJ mol^{-1} almost invariant from the collision energy. This indicates that the exit transition state from the intermediate to the reaction products is likely to be tight and hence involves a repulsive bond rupture. Last, we can calculate the fraction of total available energy channeling into translational energy of the products. If we assume the less stable C_6H_5NC isomer does not contribute to the reactive scattering signal, we find fractions of 30%–35% for all collision energies.

D. Center-of-mass angular distributions $T(\theta)$ and flux contour maps $I(\theta, u)$

At all collision energies, the $T(\theta)$ and $I(\theta,u)$ are forward–backward symmetric. This suggests that the reaction follows indirect scattering dynamics via complex formation. Further, the 0°–180° symmetry documents either a lifetime of the decomposing complex longer than its rotational period or a ''symmetric exit transition state.'' In the latter case, the rotation interconverts leaving hydrogen atoms in the decomposing complex via a proper rotation axis, and the complex fragment with equal probability in θ and $\pi-\theta$. This behavior would result in a symmetric flux distribution although the lifetime of the complex might be less than a rotational period.[33] Instead of sharp peaking of the $T(\theta)$ as shown in Figs. 7–9, the peak can be replaced by a flat plateau extending from 165° to 205° as well without a signifi-

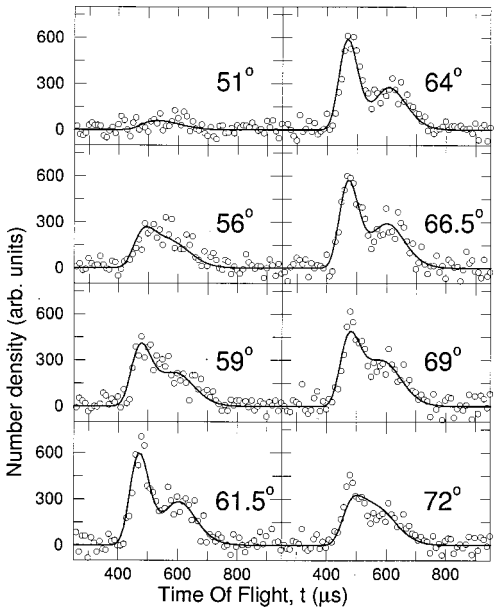

FIG. 4. Time-of-flight data of distinct laboratory angles as indicated in Fig. 1. The dots indicate the experimental data, the solid lines the calculated fit.

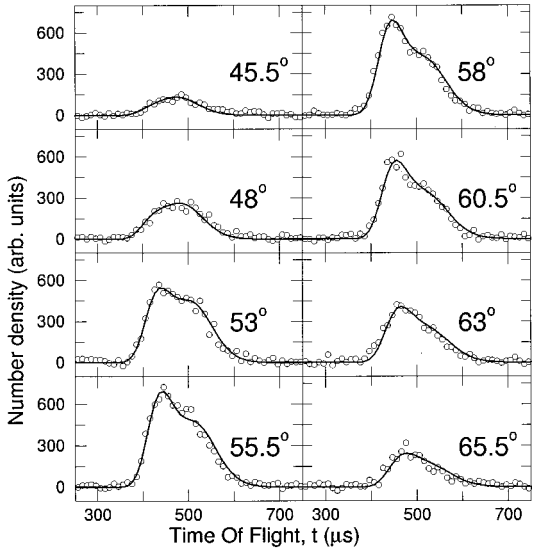

FIG. 5. Time-of-flight data of distinct laboratory angles as indicated in Fig. 2. The dots indicate the experimental data, the solid lines the calculated fit.

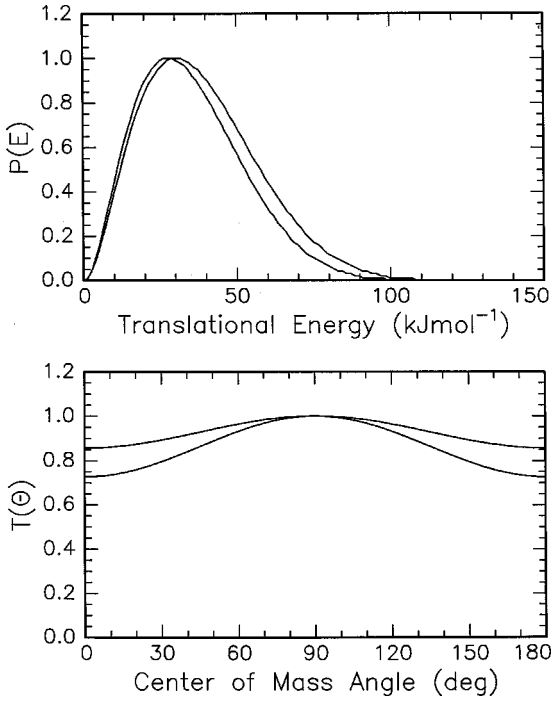

FIG. 7. Center-of-mass angular flux distribution (lower) and translational energy flux distribution (upper) for the reaction of $CN(X\,^2\Sigma^+)+C_6D_6(X\,^1A_{1g})\rightarrow C_6D_5CN(X\,^1A_1)+D(^2S_{1/2})$ at a collision energy of 19.5 kJ mol^{-1}.

cant change in the fit of our laboratory data. All $T(\theta)$s peak at $\pi/2$ with intensity ratios $I(0°)/I(90°)=0.73-0.86$, 0.50–0.56, and 0.61–0.73 from the lowest to highest collision energy. This finding documents geometrical constraints of the direction of the H/D atom emission in the decomposing C_6H_6CN/C_6D_6CN intermediates (see Sec. V). As the collision energy rises, these constraints become less pronounced in the C_6H_6/CN: if we consider the reversed reaction, i.e., an addition of an H atom to the cyanobenzene molecule, higher collision energies allow a wider range of impact parameters to react. Alternatively, an increase of the energy available to the decomposing complex and the transition state translates into more internal excitation of the cyanobenzene and therefore the departing H will have precessional motions more pronounced. We like to stress that an isotropic distribution could not fit to our experimental data. Likewise we tried a

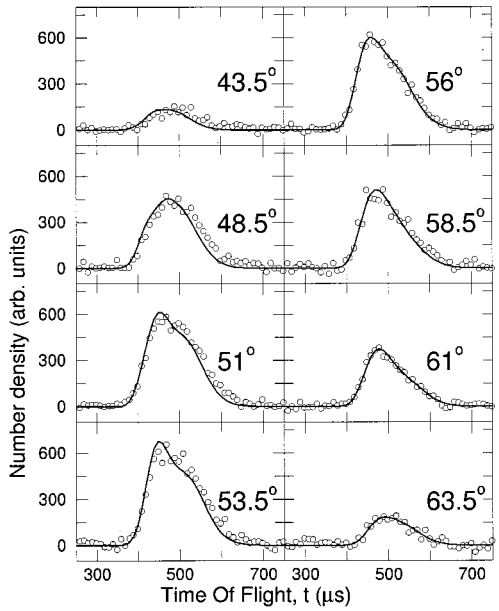

FIG. 6. Time-of-flight data of distinct laboratory angles as indicated in Fig. 3. The dots indicate the experimental data, and the solid lines indicate the calculated fit.

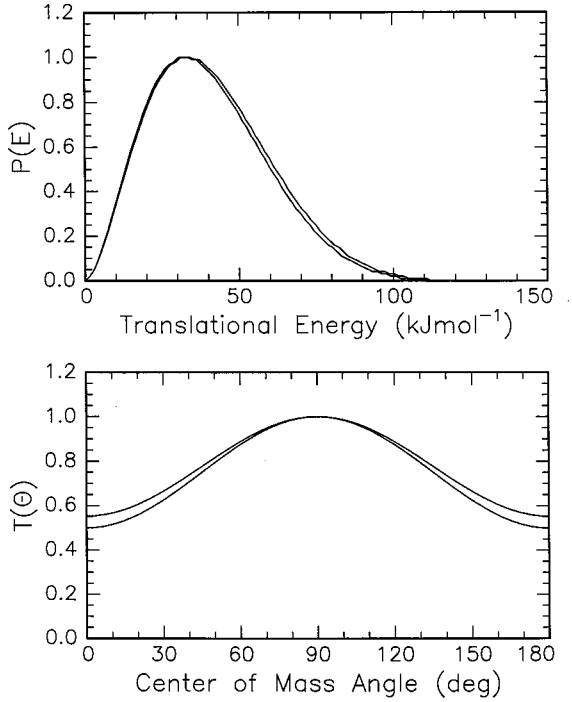

FIG. 8. Center-of-mass angular flux distribution (lower) and translational energy flux distribution (upper) for the reaction of $CN(X\,^2\Sigma^+)+C_6H_6(X\,^1A_{1g})\rightarrow C_6H_5CN(X\,^1A_1)+H(^2S_{1/2})$ at a collision energy of 30.6 kJ mol^{-1}.

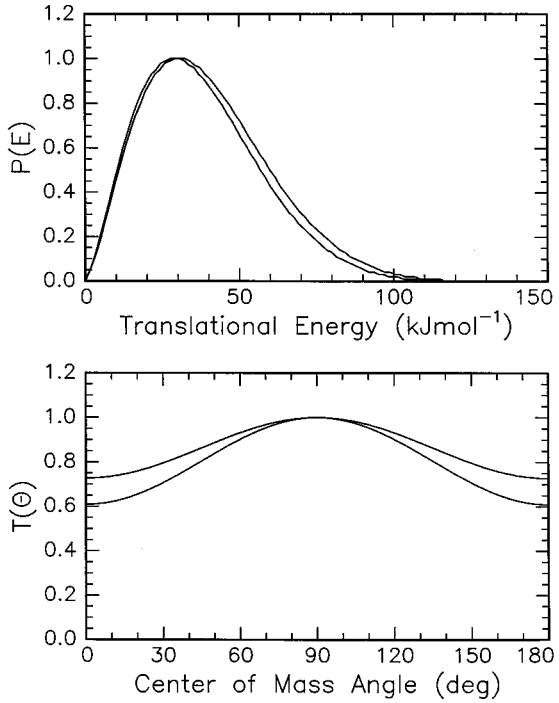

FIG. 9. Center-of-mass angular flux distribution (lower) and translational energy flux distribution (upper) for the reaction of $CN(X\,^2\Sigma^+) + C_6H_6(X\,^1A_{1g}) \rightarrow C_6H_5CN(X\,^1A_1) + H(^2S_{1/2})$ at a collision energy of 34.4 kJ mol^{-1}.

two-channel fit assuming the C_6H_5NC isomer or the C_6H_6CN adduct might be involved in the reaction. We derived upper limits of less than 2% of their contributions.

V. DISCUSSION

A. *Ab initio* C_7H_6N potential energy surface

In order to account for the experimental observation of the C_7H_5N product isomer(s), we investigated computationally the attack of the CN radical on the π electron density of the benzene molecule via C_7H_6N intermediates, (see Figs. 13–18 and Table II). The computed Mulliken spin densities indicate that the unpaired electron of the cyano radical is mainly localized on the carbon atom, making this the more reactive site in radical reactions. Indeed, the formation of the CN addition product 1-cyano-cyclohexadienyl, **1**, is significantly more exothermic (-165.4 kJ mol^{-1}) than the NC addition (-77.8 kJ mol^{-1}) to the 1-isocyano-cyclohexadienyl radical, **2**. Most important, we find a marked difference in the mechanisms yielding **1** and **2**. Both pathways involve no entrance barrier, but whereas **1** is formed from benzene and the cyano radical without a long-range complex, the reaction yielding **2** is more complex. The approach of CN via the N atom first results in the formation of a weakly bound (-17.2 kJ mol^{-1}) complex **3**. The NC moiety is separated by 254.0 pm from the closest benzene carbon atom and is oriented almost perpendicular (104.6°) to the benzene ring plane. A transition state, which is only slightly higher in energy than **3** (-13.5 kJ mol^{-1}) connects the long-range complex **3** to **2**.

The dissociation of hydrogen atoms from the tetrahedral carbons in **1** and **2** are the thermodynamically most favorable reactions of the cyclohexadienyl radicals producing the C_7H_5N isomers cyanobenzene (-94.6 kJ mol^{-1}) or iso cyanobenzene (-4.9 kJ mol^{-1}), respectively. The calculated exothermicity to the cyanobenzene isomer lies near an experimentally reported value of 84.7 ± 8 kJ mol^{-1}.[34] The barriers for these homolytic bond cleavage processes via tight transition states are very similar, 103.6 and 107.3 kJ mol^{-1} with respect to **1** and **2**, respectively. However, as **2** is significantly higher in energy than **1** (87.6 kJ mol^{-1}), the transition state to form the iso cyanobenzene isomer is located 29.5 kJ mol^{-1} above the reactants. The geometries of both exit transition states are characterized by nearly planar cyano- or iso-cyanobenzene moieties with almost perpendicularly (97.2° and 101.2°, respectively) oriented hydrogen atoms [r(CH) = 178.9 and 176.8 pm, respectively].

The ring closure reactions of **2** and **3** to yield the bicyclic radicals (see Figs. 16 and 17), provide possible alternatives to the hydrogen dissociation channels. However, the ring closure reactions are both thermodynamically significantly less favorable than the hydrogen dissociation. Whereas the cyclization product of **2**, c-C_6H_6NC, is more stable than separated benzene and CN, the cyclization product of **3**, c-C_6H_6CN, lies 162.7 kJ mol^{-1} above the reactants. Although the sequence as shown in Fig. 18 provides a route to an eight membered monocyclic C_7H_5N isomer, this pathway to an antiaromatic 8 π system is predicted to be endothermic by 318.0 kJ mol^{-1} and hence well above our highest collision energy.

Rather than attacking the π electron density, the abstraction of a hydrogen atom by the cyano radical might be anticipated as an additional, different mode of reaction. The overall reactions to yield phenyl radical plus HCN or HNC are exothermic by 74.3 and 15.7 kJ mol^{-1}, respectively. Whereas the hydrogen abstraction via the cyano carbon atom is therefore thermodynamically less favorable than the addition–elimination reaction, the abstraction is more exothermic than the substitution in the case of an NC attack.

B. Reaction pathway

1. Energetical constraints

The high-energy cutoffs of our $P(E_T)$s are in line with the formation of the cyanobenzene isomer in its $^1A_1$ electronic ground state. The experimental data suggest an exothermicity of about 77–93 kJ mol^{-1}, whereas the electronic structure calculations predict 94.6 kJ mol^{-1}. The formation of the less stable iso cyanobenzene isomer is exothermic by only 4.9 kJ mol^{-1}, and hence it can be excluded as a major contributor. A closer look at the pertinent potential energy surface supports these conclusions. The only reaction pathway to form iso cyanobenzene must proceed via the transition state connecting the products and the 1-isocyano-cyclohexadienyl radical, **2**. But this transition state is located 29.5 kJ mol^{-1} (C_6H_6/CN) and 34.5 kJ mol^{-1} (C_6D_6/CN) above the reactants. In the perdeutero case, the system cannot overcome this barrier since the collision energy of 19.0 kJ mol^{-1} is too low; hence this transition state blocks the formation of the iso cyanobenzene molecule in our C_6D_6/CN experiments. Since the experimental data at all three colli-

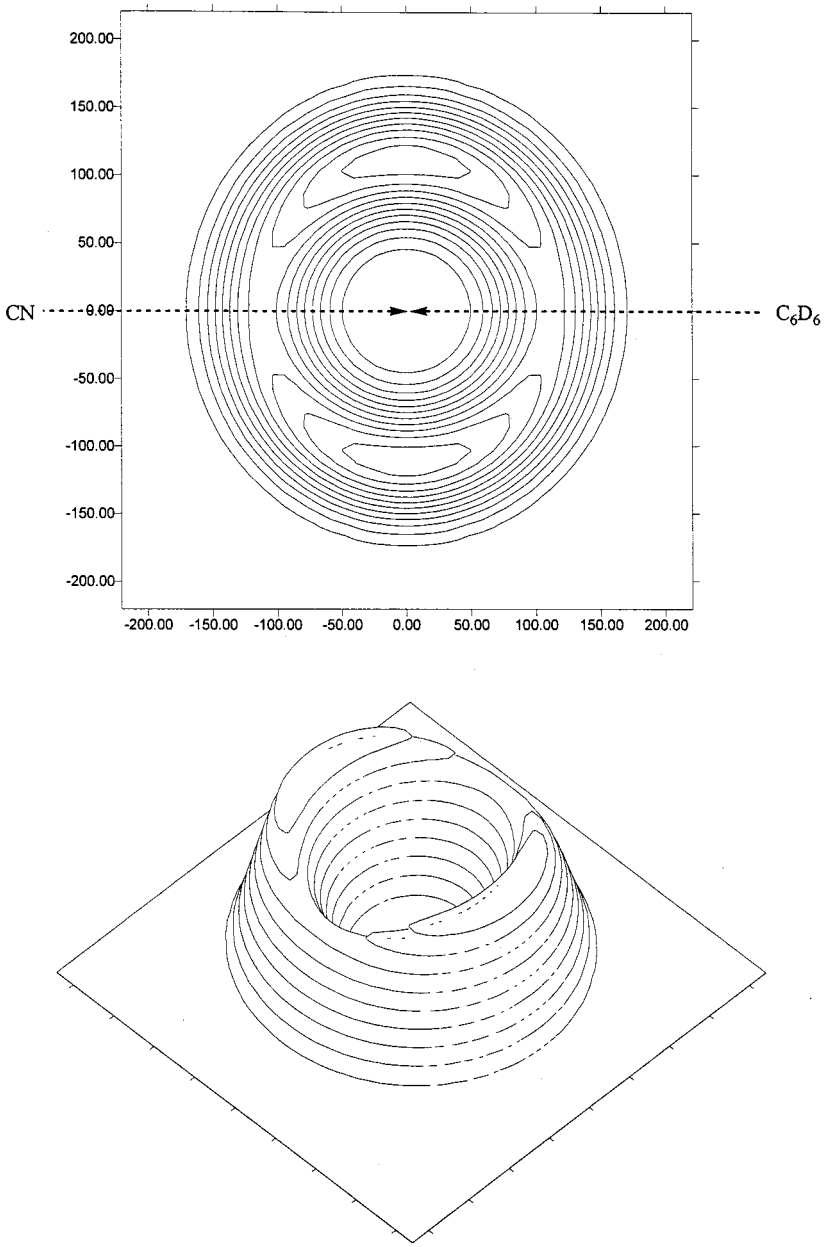

FIG. 10. Center-of-mass velocity contour flux map distribution for the reaction of $CN(X\,^2\Sigma^+) + C_6D_6(X\,^1A_{1g}) \rightarrow C_6D_5CN(X\,^1A_1) + D(^2S_{1/2})$ at a collision energy of 19.5 kJ mol^{-1}. Units are given in ms^{-1}.

sion energies could be fit with basically the same $P(E_T)$ only extended for the additional collision energy, it is very likely that the less stable iso cyanobenzene isomer does not contribute to our reactive scattering signal.

2. RRKM calculations

The calculated RRKM rate constants as compiled in Table III also support our conclusions. First, it is obvious that the 1-cyano-cyclohexadienyl adduct, **1**, cannot be detected in our experiments. Here, the lifetime of **1** is calculated to be about 4–10 ns under our experimental conditions. The adduct moves with a center-of-mass velocity between 853 and 1000 ms^{-1} at our lowest and highest collision energy, respectively. Accounting for the flight length from the interaction region to the ionizer, the adduct would need 340 and 400 μs to reach the ionizer. Therefore the lifetime of the adduct **1** is five orders of magnitude too low to survive the flight path to the ionizer. Furthermore, the RRKM lifetime for **2** of 3 ns is about three orders of magnitude larger than typical rotational periods of long-lived decomposing species which have lifetimes around 1–4 ps; hence a long-lived complex behavior results in forward–backward symmetric center-of-mass angular distributions as observed experimentally. An alternative explanation of a symmetric exit transition state which might be responsible for the forward–backward center-of-mass angular distribution can be dismissed, since the fragmenting C_6H_6CN intermediate belongs to the C_s point group and has no rotation axis.

3. The actual reaction pathway

Based on these considerations, the following chemical reaction dynamics are likely. The $CN(X\,^2\Sigma^+)$ radical attacks the π electron density in the E_{2g} highest occupied molecular orbital of the $C_6H_6(X\,^1A_{1g})$ molecule to form a carbon–carbon σ bond and a 1-cyano-cyclohexadienyl radical $(X\,^2A'')$ (**1**) without entrance barrier. Radical (**1**) belongs to

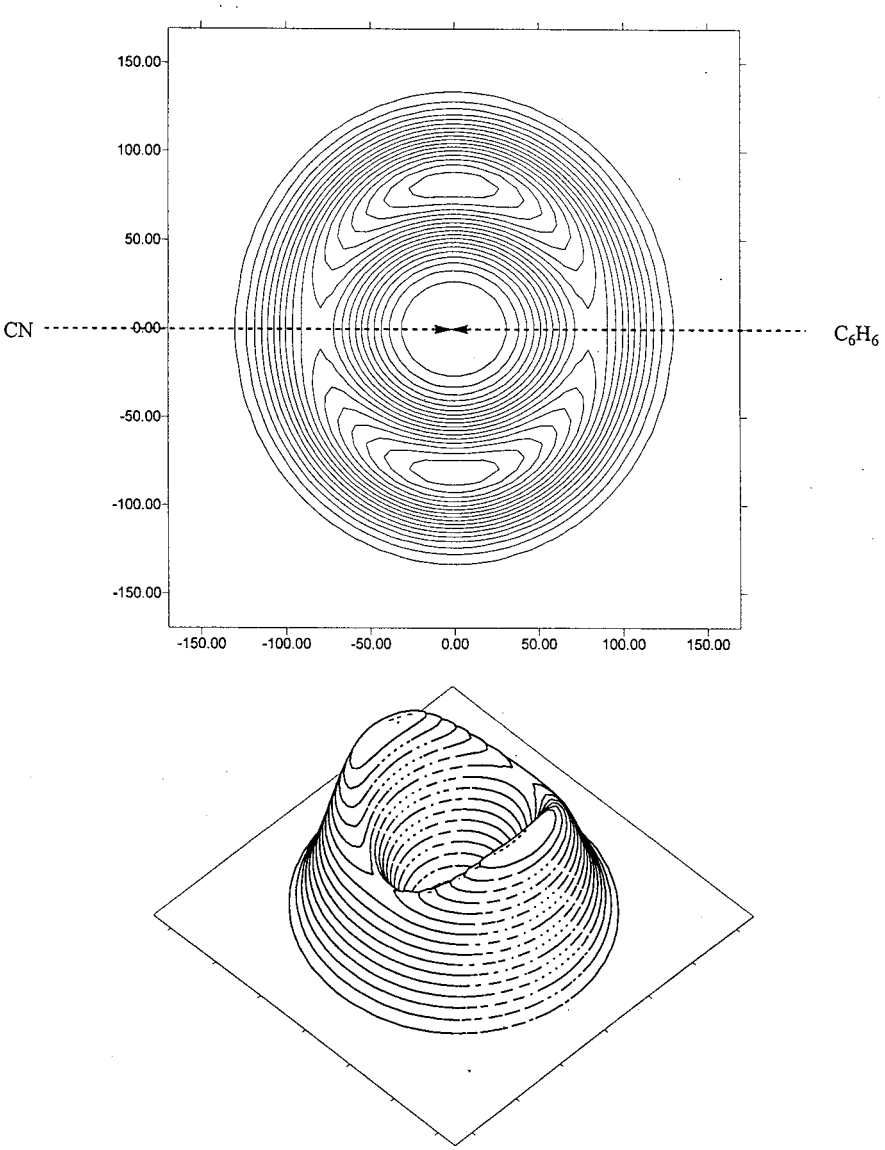

FIG. 11. Center-of-mass velocity contour flux map distribution for the reaction of $CN(X\,^2\Sigma^+)+C_6H_6(X\,^1A_{1g}) \rightarrow C_6H_5CN(X\,^1A_1)+H(^2S_{1/2})$ at a collision energy of 30.6 kJ mol^{-1}. Units are given in ms^{-1}.

the C_s point group and is bound by a calculated 165.4 kJ mol^{-1} with respect to the reactants and resembles a prolate asymmetric top. The heavy atoms are rotating nearly in plane, perpendicular to the total angular momentum vector **J** around the *C* axis. The long lived reactive intermediate (**1**) undergoes C–H bond rupture through a tight exit transition state located 34.9 kJ mol^{-1} above the products, but well below the reactants, to form a hydrogen atom and the C_{2v} symmetric cyanobenzene isomer, $C_6H_5CN(X\,^1A_1)$. As documented by the sideways peaking of the center-of-mass angular distribution and electronic structure calculations, this H atom is emitted almost perpendicular to the heavy atoms which almost form a C_6H_5CN plane with an angle of about 101.2° nearly parallel to **J** as documented; based on these findings, the C_6H_5CN product mainly rotates around the *C* axis (see Fig. 19).

C. Exit transition state and comparison with the F/C_6D_6 system

It is well established that when a long-lived complex is formed during a reaction, $T(\theta)$ is characterized by forward–backward symmetry, i.e., the angular distribution is symmetric with respect to $\theta=90°$.[35] While the symmetry is an essential requirement, the shape of the $T(\theta)$ is determined by the disposal of the total angular momentum **J** and a variety of shapes are indeed possible. In crossed beam experiments, the reactant molecules undergo a supersonic expansion and a substantial rotational cooling occurs; therefore, the total angular momentum is mainly given by the initial orbital angular momentum **L**. The products can be rotationally excited, however, so that Eq. (2) holds

$$\mathbf{J}\approx\mathbf{L}\approx\mathbf{L}'+\mathbf{j}' \tag{2}$$

with the rotational angular momenta of the products $\mathbf{j}'$, and the initial and final orbital angular momenta **L** and $\mathbf{L}'$. In Eq. (2) we made use of the fact that the nuclear momenta are much smaller than **L** and $\mathbf{L}'$. Since the unpaired electron occupies a σ molecular orbital in the cyano radical and a 1*s* atomic orbital in the H atom, the angular momentum of the electron $\mathbf{j_e}$ is zero. The final recoil velocity vector $\mathbf{v}'$ is in a plane perpendicular to $\mathbf{L}'$ and therefore, when the rotational excitation of products is significant, $\mathbf{v}'$ is not in a plane per-

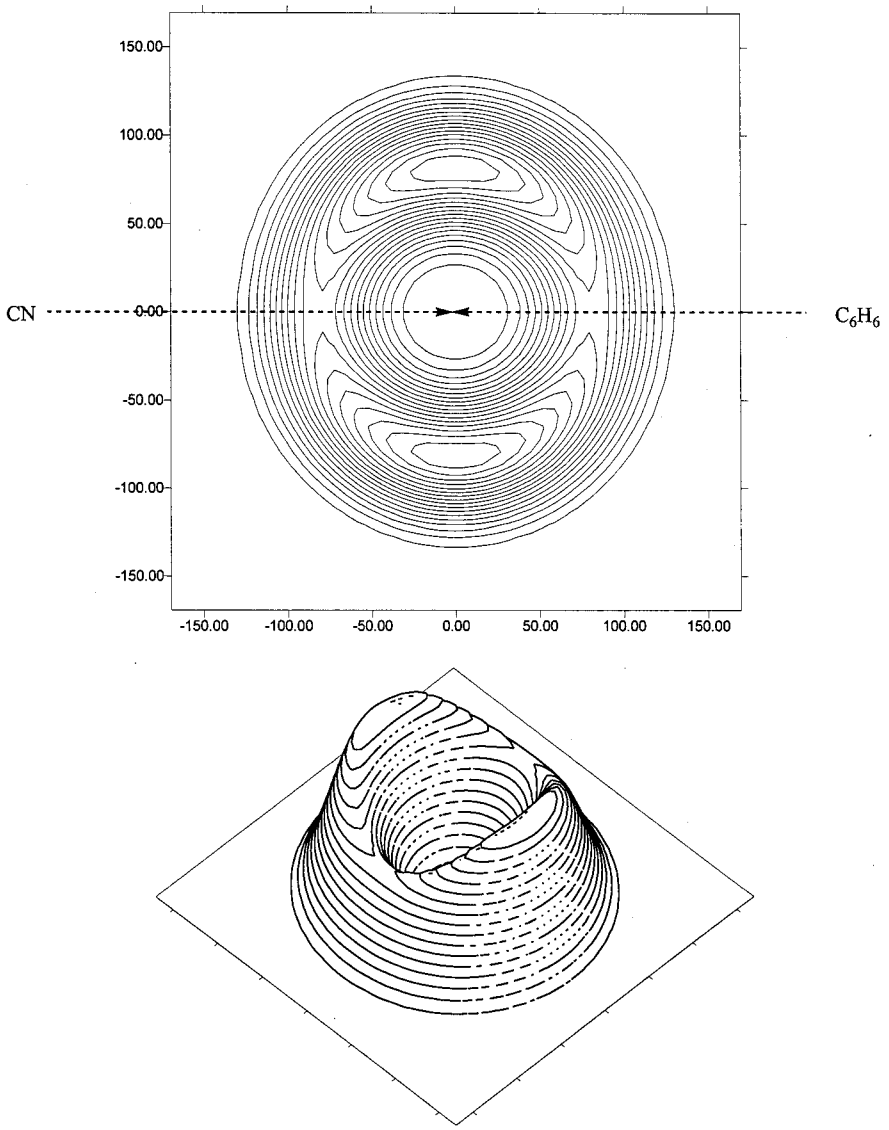

FIG. 12. Center-of-mass velocity contour flux map distribution for the reaction of $CN(X\,^2\Sigma^+)+C_6H_6(X\,^1A_{1g}) \rightarrow C_6H_5CN(X\,^1A_1)+H(^2S_{1/2})$ at a collision energy of 34.4 kJ mol^{-1}. Units are given in ms^{-1}.

pendicular to **J**. When $\mathbf{j}'$ is not zero, the probability distribution for the scattering angle θ, which is the center-of-mass angle between the initial relative velocity **v** and $\mathbf{v}'$, depends on the values of J, M, and M', where M and M' are the projections of **J** on the initial and final relative velocity, respectively. For instance, if the complex dissociates preferentially with low M' values, the final velocity $\mathbf{v}'$ is almost perpendicular to **J** and therefore $\mathbf{v}'$ and **v** are almost parallel; in this case, the product intensity will be mainly confined to the poles $\theta=0°$ and $\theta=180°$, similarly to the case of no product rotational excitation. On the contrary, when the collision complex dissociates mainly with high M' values, the final relative velocity will be almost parallel to **J** and perpendicular to **v** and the products will be preferentially scattered at $\theta=90°$. Usually, a distribution of M' values is possible; in some cases, however, the geometry of the decomposing complex may imply a most probable M' value.

In the present case, the $T(\theta)$ curves derived at three different collision energies exhibit a symmetric shape and a peaking at $\theta=90°$ suggesting that the H(D) atom is ejected more favorably in a direction close to the direction of the total angular momentum. This behavior strongly resembles what is observed for the similar reaction $F+C_6D_6 \rightarrow C_6D_5F+D$ in a crossed beam study by Lee and co-workers at a collision energy of 10.7 kJ mol^{-1}.[36] Remarkably, the experimentally determined $T(\theta)$ has been recently reproduced by means of the microcanonical transition state theory developed by Grice and co-workers.[37] This theory offers a bridge between the shape of angular distributions of reactive scattering arising from a persistent collision complex and the structure of the decomposing transition state. The model is valid in the limiting case of a direction of dissociation parallel to one of the principal rotational axes of the transition state, but it is able to give a general description also for small deviations. The effect of the transition state geometry is predicted to be stringent in the case of hydrogen displacement reactions when they involve a potential energy barrier in the exit channel. This requirement is satisfied in the case of our title reactions since our electronic structure calculations showed that an exit barrier is present. Equally relevant is the calculated geometry of the decomposing transition state where the angle formed between the leaving H atom and the

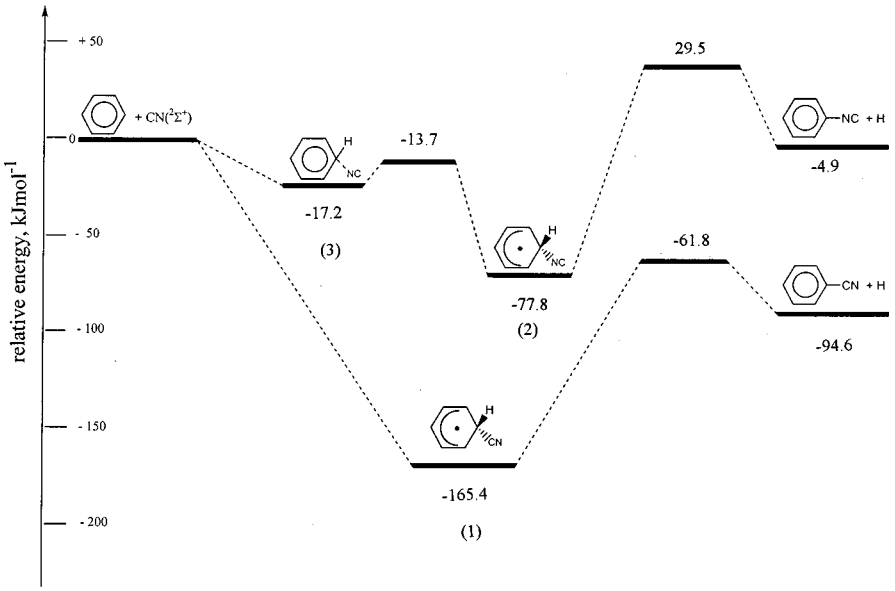

FIG. 13. Schematic representation of the C_7H_6N potential energy surface.

heavy atoms which define nearly the C_6H_5CN plane is 101.2°. In the case of $F+C_6D_6 \rightarrow C_6D_5F+D$, Smith and Grice showed that by assuming a geometry of the transition state such that the analogous angle is 90° and therefore implying a bond dissociation along the *C* axis, the experimental angular distribution by Shobatake *et al.* is perfectly reproduced within the model. The structure of the transition state was not known and the substantial coincidence of the model prediction with the experimental results offered an insight into the geometry of the transition state. In conclusion, we can say that in our case the calculated geometry of the transition state can well account for the observed sideways scattering properties. Since the CN radical is isolobal to the F atom, the title reaction is expected to show chemical dynamics similar to those of the $F+C_6D_6 \rightarrow C_6D_5F+D$ reaction. In the case of the center-of-mass angular distributions this is clearly the case.

In the analogous F reaction, the $P(E_T)$ peaks at 30 kJ mol^{-1}. The position of the flux distribution maximum is very similar to those of the $CN+C_6H_6/C_6D_6$ reactions, i.e., 28–35 kJ mol^{-1}. This suggest similar dynamics in the exit channel of both reactions to the H/D atom loss and the reversed reactions, i.e., the addition of a H/D atom to the C_6H_5X (X=F, CN) molecule via an entrance barrier of the same order of magnitude. However, the fraction of energy

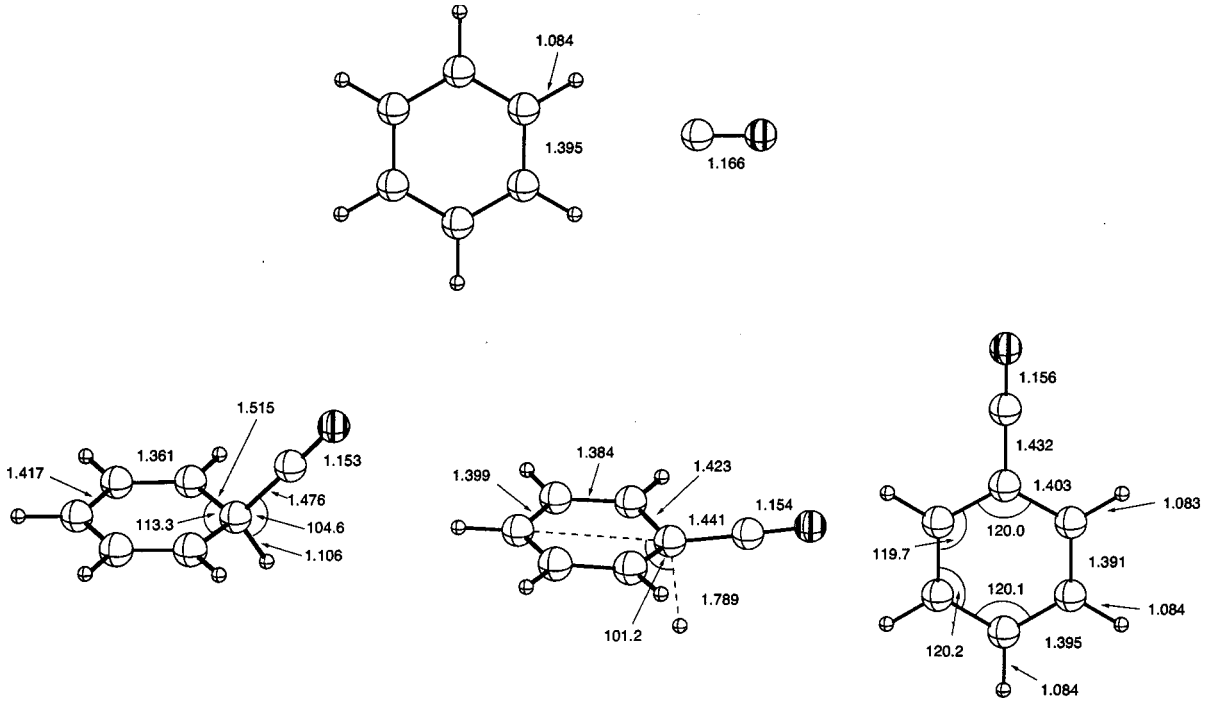

FIG. 14. Bond distances in Angstrom and bond angles in degrees for reactants, intermediates, transition states, and products leading to the formation of cyanobenzene.

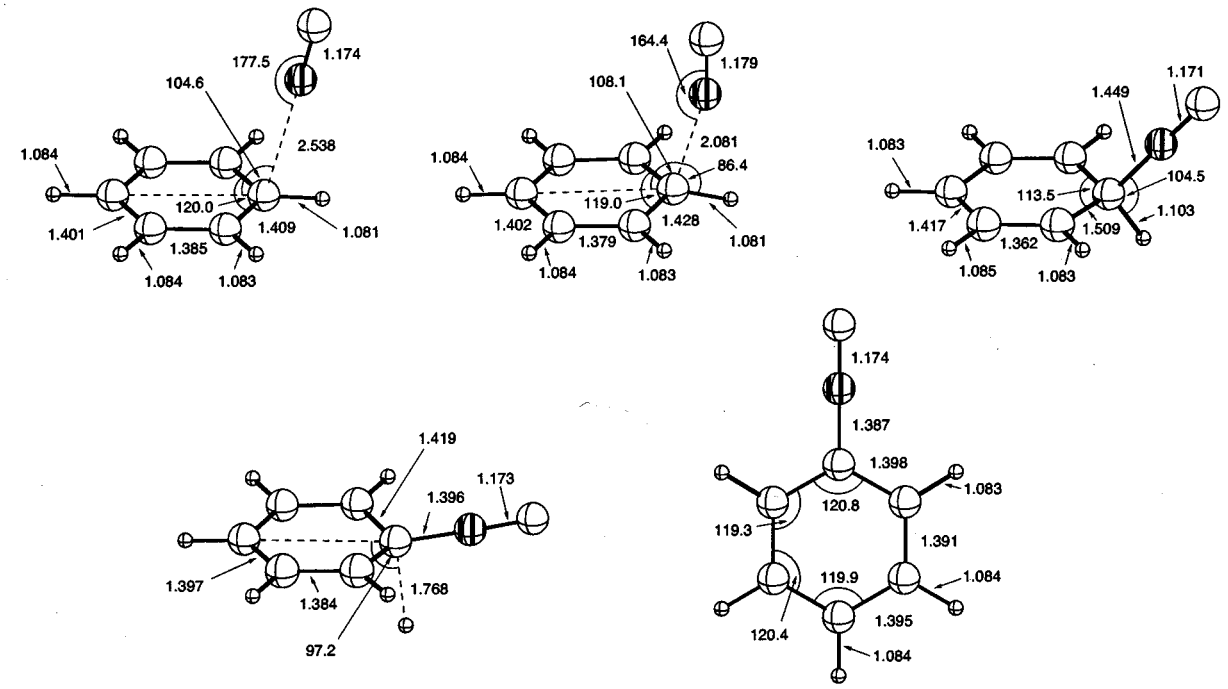

FIG. 15. Bond distances in Angstrom and bond angles in degrees for intermediates, transition states, and products leading to the formation of iso cyanobenzene.

released as translation depicts a marked difference in the two reactions. Whereas 45% of the available energy channels into translational of the C_6D_5F+D products, our title reaction gives only 30%–35%. This is likely based on the lower bending modes of the decomposing intermediate and the transition state in the title reaction as compared to the F/C_6D_6 system. Further, the additional atom increases the vibrational degrees of freedom by 3. This could result in an enhanced internal energy compared to the $F+C_6D_6$ reaction.

VI. IMPLICATIONS FOR INTERSTELLAR CHEMISTRY

The CN radical is ubiquitous in interstellar clouds like the Taurus Molecular Cloud 1 Orion Molecular Cloud, and the outflow of old, dying carbon stars such as IRC+10126.[36] Based on bulk experiments on the reactions of cyano radicals with unsaturated hydrocarbons as described in Sec. I, it has been postulated that rapid neutral–neutral reactions might be involved in the synthesis of nitriles and/or iso nitriles in these extraterrestrial environments,[13] among them unsaturated cyanopolyines $H-(CC)_n-CN$ ($n=1-5$), C_5N, and C_3N to name a few. However, these experiments monitored the decay kinetics of the CN radical, and therefore the products could not be determined experimentally.

The present experiments clearly show that the reaction of benzene with the cyano radicals only forms cyanobenzene and not the iso cyanobenzene isomer. Although benzene has never been observed in the interstellar medium, chemical models of interstellar clouds and carbon rich outflows predict fractional abundances of about 10^{-8} relative to H_2. The crucial observational drawback is the lack of a permanent benzene dipole moment which is essential for a radio astronomical observation in the gas phase. Our findings suggest that since the title reaction is barrierless and exothermic, prospective radio astronomical searches should focus on the

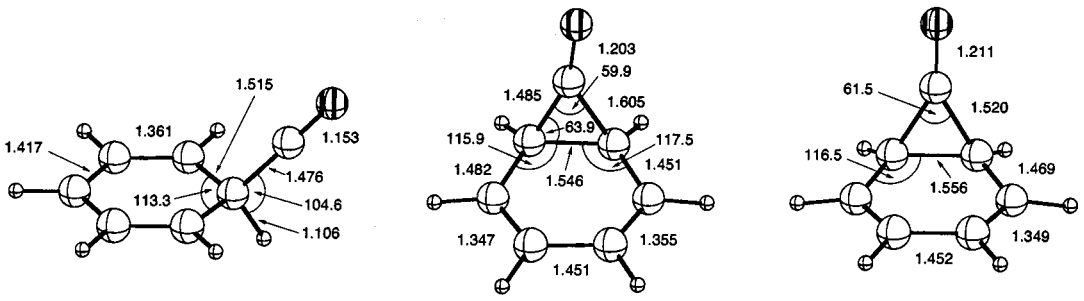

FIG. 16. Bond distances in Angstrom and bond angles in degrees for the cyclization of the C_6H_6CN intermediate.

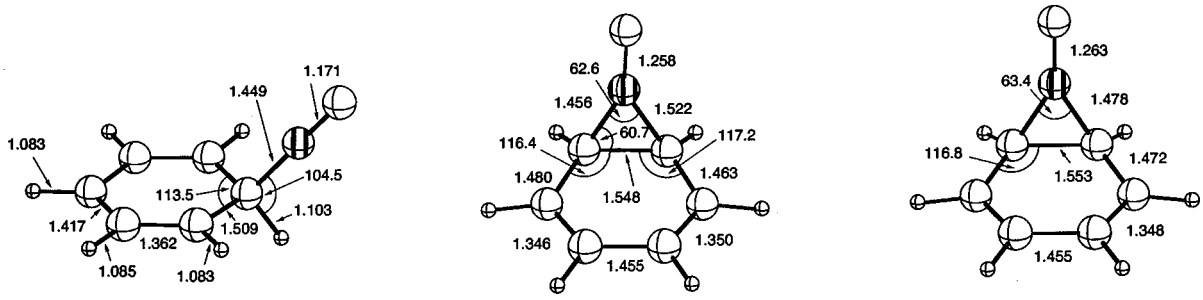

FIG. 17. Bond distances in Angstrom and bond angles in degrees for the cyclization of the C_6H_6NC intermediate.

C_6H_5CN isomer in those areas where CN radicals have been clearly identified and where chemical reaction models predict cyanobenzene formation. So cyanobenzene could act as a tracer molecule for benzene in the interstellar medium.

In addition, the reaction of CN radicals with benzene could be a crucial step in the synthesis of heteroatom polycyclic aromatic hydrocarbons (PAHs). Here, all postulated pathways to PAH formation in the gas phase of interstellar environments involve either benzene or the phenyl radical C_6H_5.[38] The crucial and limiting step in these reaction networks, however, is the collision of C_2H radicals with benzene. A detailed model investigation shows that this reaction is only feasible in a very narrow temperature window between 1200 and 1300 K. The title reaction, however, is exothermic and holds no entrance barrier. Therefore, C_5H_5CN molecules could be formed even at temperatures as low as 10 K. We would like to stress that the CN radical does not destroy the aromatic skeleton as atomic carbon $C(^3P_j)$ does.[39]

VII. IMPLICATIONS FOR SOLAR SYSTEM CHEMISTRY

Besides interstellar chemistry, the chemical dynamics of $CN(X\,^2\Sigma^+)$ radical reactions with unsaturated hydrocarbons are of fundamental relevance to the atmospheric chemistry in Saturn's moon Titan.[40] Titan's atmospheric composition is dominated by N_2 and CH_4 together with the minor components C_2H_6, C_3H_8, C_2H_2, HCN, HC_3N, CH_3CCH, and C_2N_2.[41,42] Titan's cyano chemistry is thought to be initiated by photolysis of HCN and C_2N_2 by solar radiation to generate reactive CN radicals in their $^2\Sigma^+$ electronic ground state. These radicals could react with benzene in Titan's atmosphere. Although cyanobenzene has not been observed yet, the unsaturated nitriles cyano acetylene HCCCN, acrylonitrile C_2H_3CN, and cyanopropyne CH_3CCCN have been observed unambiguously. Therefore, our results offer a challenging mission for the NASA-ESA Cassini–Huygens spacecraft to Titan.[43] The Huygens mission will carry an IR mapping spectrometer as well as a quadrupole mass spectrometer capable of identifying these isomers in Titan's atmosphere.[14]

VIII. CONCLUSIONS

The crossed molecular beam experiments together with electronic structure calculations and RRKM studies show that the radical–neutral reaction of the cyano radical $CN(X\,^2\Sigma^+)$ with benzene $C_6H_6(X\,^1A_{1g})$ is initially dominated by long-range dispersion forces. The reaction is barrierless and is governed by an initial attack of the CN radical

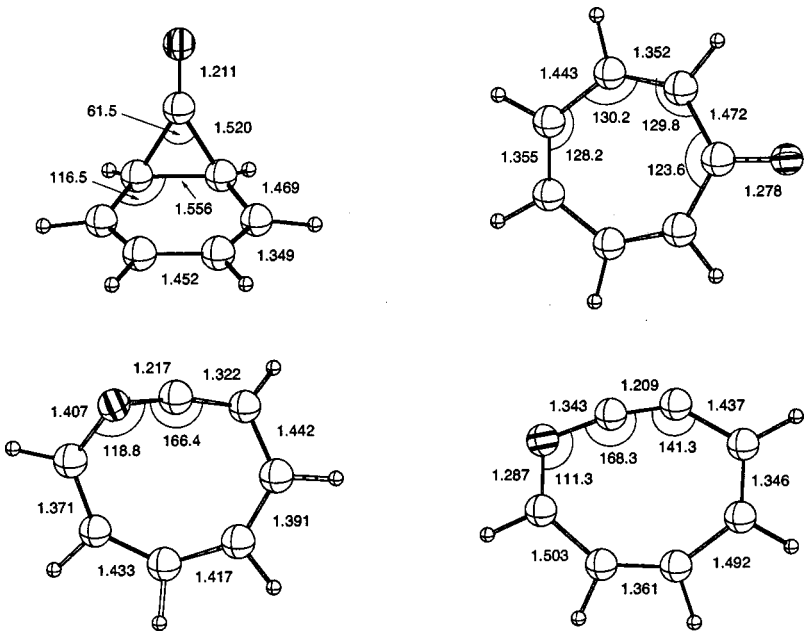

FIG. 18. Bond distances in Angstrom and bond angles in degrees for involved intermediates in the rearrangement of the C_6H_6CN intermediate to *N*-cyclooctyne-2.

TABLE II. Electronic states, dipole moments μ (D), and rotational constants *A*, *B*, and *C* (GHz) of various molecules at the B3LYP/6-311+G** level of theory.

Species	Electronic state	μ	*A*	*B*	*C*
C_6H_6	$^1A_{1g}$	0	5.704	5.704	2.852
CN	$^2\Sigma_g$	1.4	0.0	57.533	57.533
HCN	$^1\Sigma_g$	3.1	0.0	44.763	44.763
HNC	$^1\Sigma_g$	3.1	0.0	45.418	45.418
C_6H_5	$^2A_1$	0.9	6.295	5.619	2.969
C_6H_6CN	$^2A'$	4.2	4.529	1.621	1.304
C_6H_5CN	$^1A_1$	4.7	5.672	1.549	1.216
C_6H_6•••NC	^1A	4.2	3.518	1.400	1.272
C_6H_6NC	$^2A'$	4.1	4.566	1.697	1.352
C_6H_5NC	$^1A_1$	4.1	5.679	1.637	1.270
c-C_6H_6NC	$^2A''$	4.8	3.753	2.243	1.787
c-C_6H_6CN	$2A''$	4.1	3.765	2.116	1.708

with the carbon atom to the aromatic π electron density of the benzene molecule to form a C_s symmetric C_6H_6CN collision complex. At all collision energies, the center-of-mass angular distributions are forward–backward symmetric and show a peaking at $\pi/2$, documenting that the decomposing complex has a lifetime longer than its rotational period, and that the light hydrogen atom is emitted almost perpendicular to the C_6H_5–CN plane resulting in a sideways scattering. This finding is strongly supported by our electronic structure calculations depicting a H–C–C angle in the exit transition state of 101.2°. This results in a peaking of the center-of-mass angular distribution at $\pi/2$. As the collision energy rises, the exit transition state geometry is less constrained, and the intensity of the center-of-mass angular distribution at the poles compared to $\pi/2$ decreases. The exit transition state is found to be tight and located about 34.9 kJ mol^{-1} above the products. Our experimentally determined reaction exothermicity of 70–90 kJ mol^{-1} is in good agreement with 94.6 kJ mol^{-1} obtained at the B3LYP/6-311+G**+ZPVE level of theory. The identification of the cyanobenzene strongly supports the inclusion of the title reaction in reaction networks modeling the chemistry in dark molecular clouds, the outflow of dying carbon stars, hot molecular cores, as well as the atmosphere of hydrocarbon rich planets and hydrocarbon-rich satellites such as Saturn's moon Titan. This process might further contribute to the formation of heteroatomic PAHs in these extraterrestrial environments as well as hydrocarbon flames via cyanobenzene.

TABLE III. RRKM rate constants in units of s^{-1}. Tunneling corrections were applied for k_2.

Collision energy	0 kJ mol^{-1}	19.5 kJ mol^{-1}	30.6 kJ mol^{-1}	34.4 kJ mol^{-1}
k_1 [a]	1.27*E*10	1.97*E*10	2.29*E*10	2.39*E*10
k_{-1} [b]	2.83*E*6	7.44*E*7	2.439*E*8	3.43*E*8
k_2 [c]	n.r.[e]	n.r.[e]	2.46*E*3	6.77*E*3
k_3 [d]	2.43*E*7	2.05*E*8	2.08*E*8	2.59*E*8

[a] k_1 = from (3) to (2).
[b] k_{-1} = from (2) to (3).
[c] k_2 = from (2) to C_6H_5NC+H.
[d] k_3 = from (1) to C_6H_5CN+H.
[e] n.r. = no reaction.

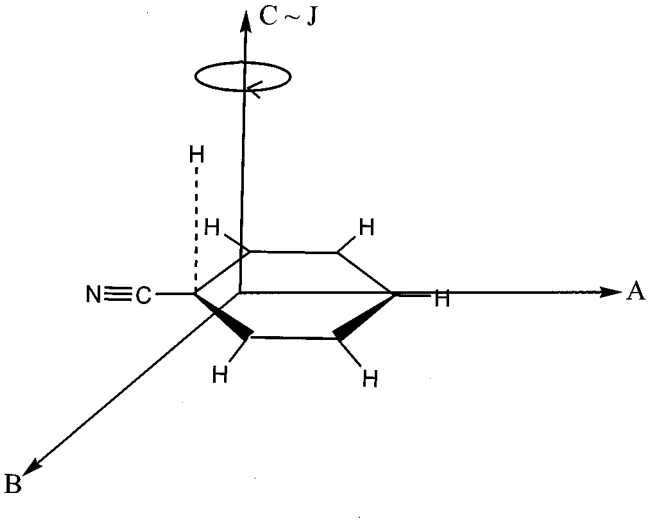

FIG. 19. Schematic representation of the decomposing C_6H_6CN complex, rotation axes *A*, *B*, and *C*, together with the total angular momentum vector **J**.

ACKNOWLEDGMENTS

R.I.K. is indebted the Deutsche Forschungsgemeinschaft (DFG) for a *Habilitation* fellowship (Grant No. IIC1-Ka1081/3-1) and Professor D. Gerlich (Technical University Chemnitz, Germany) for support. The work was further supported by Academia Sinica and the Taiwanese Petrol Organization. The work in Athens was supported by the U.S. Department of Energy.

[1] R. D. Kern, K. Xie, and H. Chen, Combust. Sci. Technol. **85**, 77 (1992); G. J. Collin, H. Deslauriers, G. R. De Mare, and R. A. Poirier, J. Phys. Chem. **94**, 134 (1990); P. R. Westmoreland, A. M. Dean, J. B. Howard, and J. P. Longwell, *ibid.* **93**, 8171 (1989), and references therein; G. Rotzell, Int. J. Chem. Kinet. **17**, 637 (1985); R. D. Smith, Combust. Flame **35**, 179 (1979).
[2] R. I. Kaiser, D. Stranges, Y. T. Lee, and A. G. Suits, Astrophys. J. **477**, 982 (1997).
[3] Y. T. Lee, Science **236**, 793 (1987).
[4] J. H. Wang, K. Liu, G. C. Schatz, and M. ter Horst, J. Chem. Phys. **197**, 7869 (1997).
[5] D. M. Sonnenfroh, R. G. MacDonald, and K. Liu, J. Chem. Phys. **93**, 1478 (1990).
[6] M. Alagia, N. Balucani, P. Casavecchia, D. Stranges, and G. G. Volpi, J. Chem. Soc., Faraday Trans. **91**, 575 (1995).
[7] P. Casavecchia, N. Balucani, and G. G. Volpi, in *The Chemical Dynamics and Kinetics of Small Radicals*, edited by K. Liu and A. F. Wagner (World Scientific, Singapore, 1995), p. 365.
[8] R. G. MacDonald and K. Liu, J. Chem. Phys. **93**, 2431 (1990).
[9] G. N. Robinson *et al.*, J. Chem. Phys. **89**, 6744 (1988).
[10] R. I. Kaiser, O. Asvany, Y. T. Lee, H. Bettinger, P. V. Schleyer, and H. F. Schaefer (unpublished).
[11] R. I. Kaiser, W. Sun, A. G. Suits, and Y. T. Lee, J. Chem. Phys. **107**, 8713 (1997).
[12] R. I. Kaiser, C. Ochsenfeld, D. Stranges, M. Head-Gordon, and Y. T. Lee, J. Chem. Soc. Faraday Discuss. **109**, 183 (1998).
[13] I. Cherchneff and A. E. Glassgold, Appl. J. **419**, L41 (1993); D. A. Howe and T. J. Millar, Mon. Not. R. Astron. Soc. **244**, 444 (1990).
[14] F. Raulin *et al.*, Adv. Space Res. **22**, 353 (1998).
[15] I. R. Sims *et al.*, Chem. Phys. Lett. **211**, 461 (1993); I. W. M. Smith, I. R. Sims, and B. R. Rowe, Chem.-Eur. J. **3**, 1925 (1997).
[16] G. E. Bullok and R. Cooper, Trans. Faraday Soc. **67**, 3258 (1971).
[17] L. C. L. Huang, Y. T. Lee, and R. I. Kaiser, J. Chem. Phys. **110**, 7119 (1999).
[18] Y. T. Lee, J. D. McDonald, P. R. LeBreton, and D. R. Herschbach, Rev. Sci. Instrum. **40**, 1402 (1969).

[19] R. I. Kaiser and A. G. Suits, Rev. Sci. Instrum. **66**, 5405 (1995).
[20] R. I. Kaiser *et al.*, Rev. Sci. Instrum. (in press).
[21] D. Proch and T. Trickl, Rev. Sci. Instrum. **60**, 713 (1989).
[22] G. A. Bird, Phys. Fluids **19**, 1486 (1976).
[23] J. H. Batey, Vacuum **37**, 659 (1987).
[24] G. O. Brink, Rev. Sci. Instrum. **37**, 857 (1966).
[25] N. R. Daly, Rev. Sci. Instrum. **31**, 264 (1960).
[26] We like to point out that the thoriated iridium filament gives background counts at $m/e=191/193$ (Ir^{+}), 95.5/96.5 (Ir^{++}), 63.7/64.3 (Ir^{+++}), 47.75/48.25 (Ir^{++++}), 232 (Th^{+}), 116 (Th^{++}), and 77.3 (Th^{+++}) as detected in our experimental setup.
[27] M. S. Weis, Ph.D. thesis, University of California, Berkeley, 1986; M. Vernon, thesis, University of California, Berkeley, 1981.
[28] A. D. Becke, J. Chem. Phys. **98**, 5648 (1993).
[29] C. Lee, W. Yang, and R. G. Parr, Phys. Rev. B **37**, 785 (1988).
[30] M. J. Fritsch *et al.*, GAUSSIAN 94, Revision C.3.
[31] H. Eyring, S. H. Lin, and S. M. Lin, *Basic Chemical Kinetics* (Wiley, New York, 1980).
[32] W. H. Miller, J. Am. Chem. Soc. **101**, 6810 (1979).
[33] R. I. Kaiser, C. Ochsenfeld, M. Head-Gordon, and Y. T. Lee, Science **274**, 1508 (1996).
[34] Handbook of Chemistry and Physics (Chemical Rubber Company, Boca Raton, 1994).
[35] In theory, a deviation from this forward–backward symmetry can happen if energy conservation excludes higher *M* states. W. B. Miller, S. A. Safron, and D. R. Herschbach, Discuss. Faraday Soc. **44**, 108 (1967).
[36] K. Sobatake, J. M. Parson, Y. T. Lee, and S. A. Rice, J. Chem. Phys. **59**, 1427 (1973).
[37] R. Grice, Faraday Discuss. Chem. Soc. **124**, 381 (1988).
[38] I. Cherchneff and J. R. Barker, Ap.J. **394**, 703 (1992); R. Keller and E. Sedlmayr, Mitt. Astron. Ges. **60**, 329 (1987); I. Cherchneff, J. R. Barker, and A. G. G. M. Tielens, Ap.J. **377**, 541 (1992); M. Frenklach and E. D. Feigelson, *ibid.* **341**, 372 (1989).
[39] R. I. Kaiser *et al.*, J. Chem. Phys. **110**, 6091 (1999).
[40] D. W. Clarke and J. P. Ferris, Origins Life Evol. Biosphere **27**, 225 (1997); ESA Special Publication SP—338 Symposium on Titan (1992).
[41] B. Letourneur and A. Coustenis, Planet. Space Sci. **41**, 393 (1993).
[42] F. Raulin *et al.*, Adv. Space Res. **22**, 353 (1998).
[43] D. W. Clarke and J. P. Ferris, Icarus **115**, 119 (1995); **115**, 119 (1995).